Journal of The Electrochemical Society, **148** (11) C726-C732 (2001)
0013-4651/2001/148(11)/C726/7/$7.00 © The Electrochemical Society, Inc.

Analysis of Current-Potential Hysteresis during Electrodeposition of Copper with Additives

Kurt R. Hebert*,z

Department of Chemical Engineering, Iowa State University, Ames, Iowa 50011, USA

Two models are described for cyclic voltammetry during electrodeposition of copper from an acid sulfate bath containing the additives polyethylene glycol (PEG), chloride ions, and mercapto-1-propanesulfonate (MPSA). The same bath may be used for superfilling of cavities during fabrication of copper on-chip metallization. Experimental current-potential scans show a characteristic hysteresis in solutions with all three additives, which demonstrates the presence of both activated and inhibited kinetics. Both models assume that deposition is inhibited by a PEG-chloride adsorbed surface complex, as established previously. One model further hypothesizes that PEG is incorporated into grain boundaries in the copper at the same fractional coverage found on the external surface. The second model neglects PEG incorporation, but assumes that adsorbing MPSA directly displaces PEG from the surface. Both models predict hysteresis quantitatively similar to experiments, without the use of fitting parameters. The competitive adsorption model is favored because, unlike the PEG incorporation model, it yields realistic predictions of carbon and sulfur concentrations in the deposit.
© 2001 The Electrochemical Society. [DOI: 10.1149/1.1408634] All rights reserved.

Manuscript submitted March 26, 2001; revised manuscript received July 5, 2001. Available electronically September 28, 2001.

The damascene process for fabrication of copper on-chip metal interconnects requires electrodeposition into two- or three-dimensional cavities (trenches or vias) with width dimensions on the order of 100 nm.[1] To obtain void-free deposits, superconformal deposition, or superfilling, is necessary. These terms refer to the occurrence of more rapid electrodeposition in the bottom of the cavity than toward its entrance. Superconformal deposition is only obtained in the presence of certain combinations of additives in the plating bath. Several simulations of filling of various size cavities have appeared in the literature, which have mathematically described the effect of additives on electrodeposition.[1-10] One of the additives is assumed to adsorb on the copper surface and inhibit deposition by a site-blockage mechanism. Calculations of the deposition rate based on fundamentals would require knowledge of kinetics of adsorption as well as of processes through which the adsorbed inhibitor is consumed, such as incorporation in the deposit,[2] cathodic reduction,[5] or displacement by competitive adsorption.[8,10,11] However, an empirical approach to modeling has been followed, owing to limited fundamental information about these phenomena.

Experimental investigations of the chemical mechanism of deposition with additives are complicated by the multicomponent additive mixtures necessary to obtain superfilling. Among those studies available in the open literature, Moffat *et al.* showed that baths with three additives can be used to achieve superfilling in submicrometer cavities.[12] These were a polyether (polyethylene glycol, PEG), chloride ions, and a thiol (3-mercapto-1-propanesulfonate, MPSA). The effect of PEG has been elucidated by a kinetic study of deposition in chloride-only and PEG-chloride baths,[13] and a quartz crystal microbalance (QCM) investigation of PEG adsorption.[14] The results showed that in the presence of chloride, PEG functions as an inhibitor for deposition, adsorbing at high coverage and blocking sites for cupric ion adsorption. The thiol has been proposed to adsorb competitively with the inhibitor.[8-11] Copper films formed in baths used in the damascene process consist of very small grains on the order of 100 nm in width.[15-18] A microstructural study of deposits using a focused ion beam microscope suggested that the thiol may also act as a grain refiner, since the grain size is increased at smaller brightener concentrations.[16]

Cyclic voltammetry experiments during deposition of blanket copper films revealed current-potential (I-E) hysteresis,[8-12] as shown in Fig. 1.[12] The hysteresis is unusual, in that the cathodic deposition current is smaller in the initial cathodic scan than in the return anodic scan. No hysteresis was found in baths with fewer than the three components needed for superfilling, suggesting a correspondence between I-E hysteresis and superfilling. The width of the hysteresis loop along the potential axis expands as the thiol concentration is decreased.[8-10] Hysteresis evidently results from transient changes of the surface coverage of PEG, reflecting a transition between ''active'' and ''inhibited'' states for deposition. This activated deposition may correspond to the acceleration of plating rate observed during bottom-up filling of cavities.[8-11] It has been hypothesized to be due to slow adsorption of PEG hindered by thiol,[9] or to slow adsorption of the thiol, displacing PEG.[8,10,11]

The cyclic voltammetry experiments may be used to evaluate fundamental models for additive adsorption and consumption. Such models would facilitate prediction of deposit shape evolution in trench and via filling. In the present work, two different models for additive consumption are presented and used to simulate cyclic voltammetry experiments. They are based on distinct hypotheses for adsorbed inhibitor consumption: incorporation into the deposit and displacement by adsorbed thiol. Both simulations are developed from the kinetic model previously established for PEG-chloride baths.[13] While both treatments contain important assumptions, all

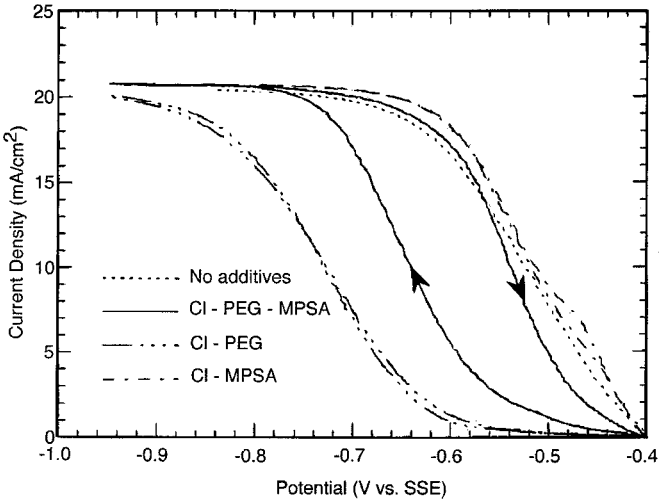

Figure 1. Experimental cyclic I-E curves for copper deposition in chloride-PEG, chloride-MPSA, and chloride-PEG-MPSA baths. Also shown is an I-E curve for a solution with no additives, obtained from a single potential sweep in the cathodic direction. The voltage scan rate was 1 mV/s. From Ref. 12. Reprinted with permission of the *Journal of The Electrochemical Society.*

* Electrochemical Society Active Member.
z E-mail: krhebert@iastate.edu

Downloaded on 2014-02-10 to IP 129.186.176.91 address. Redistribution subject to ECS license or copyright; see ecsdl.org/site/terms_use

rate equations are obtained from independent sources in which the parameters are specified. In contrast, other models for the I-E curves required curve fitting of important adsorption and deposition rate parameters.[8-10] The absence of added empiricism in the present approach facilitates the critical evaluation of the model assumptions. Also, while the empirical models have had success in the simulation of superfilling, it is likely that only fundamentally based models will ultimately be useful for exploring various plating bath compositions for the purpose of process optimization.

Mathematical Model

General considerations.—The incorporation and competitive adsorption models differ in the methods used to calculate the surface coverage of the PEG inhibitor. In this section, the equations common to both models are presented, and in the two subsequent sections, the treatments of PEG specific to each model are described.

The simulation is intended to describe linear sweep voltammetry experiments, like those in Ref. 12. Copper deposition proceeds via two consecutive irreversible reaction steps[19-21]

$$Cu^{+2}(aq) + e^- \rightarrow Cu^+(ads) \quad [1]$$

$$Cu^+(ads) + e^- \rightarrow Cu \quad [2]$$

The rate expressions for Reactions 1 and 2 are taken from Ref. 13. They are

$$r_1 = k_1 e^{-b_1 E} C_1|_{x=0}(1 - \theta_2 - \theta_3) \quad [3]$$

$$r_2 = k_2 e^{-b_2 E}\theta_3 \quad [4]$$

where $x = 0$ refers to the copper surface. The site-blocking effect of PEG is manifested in Eq. 3. In the cyclic voltammetry experiment, the applied potential is $E = E_1 - V_R t$ when $t < t_R$, the scan reversal time, and $E = E_1 + V_R(t - 2t_R)$ for $t \geqslant t_R$. Ohmic potential drop in the solution is neglected in Eq. 3 and 4, because of the presence of the highly conductive 1.8 M H_2SO_4 supporting electrolyte.

Calculation of the deposition rate from Eq. 3 and 4 requires knowledge of PEG and cuprous ion surface coverages, and the concentration of cupric ions in solution near the surface. During the voltammetry experiment, the concentration profiles of dissolved species relax to linear profiles in times on the order of the δ_i^2/D_i, where δ_i and D_i are the diffusion layer thickness and diffusivity of species i. For cupric ions, this time scale is about 30 s,[12] much smaller than the time of 900 s elapsed during the voltage scan. The Cu^{+2} concentration profile is then taken to be linear, so that its concentration at the electrode surface is

$$C_1|_{x=0} = C_{b1} - \left(\frac{\delta_1 k_1}{D_1}\right) C_1\Big|_{x=0} e^{-b_1 E}(1 - \theta_2 - \theta_3) \quad [5]$$

The adsorbed Cu^+ ion coverage is determined by a surface mole balance with generation and removal terms corresponding to Eq. 1 and 2

$$N_{s3}\frac{d\theta_3}{dt} = k_1 e^{-b_1 E} C_1|_{x=0}(1 - \theta_2 - \theta_3) - k_2 e^{-b_2 E}\theta_3 \quad [6]$$

PEG incorporation model.—In this model, the coverage of PEG is determined by a surface mole balance taking into account incorporation into the deposit. Additives within electrodeposited films have been detected by chemical analysis,[22-26] and inferred from hardness measurements and microstructural characterizations.[17,27-30] One set of chemical measurements detected carbon mole fractions as high as the order of 10^{-3}, although the concurrent detection of sulfur suggested the thiol as a possible source.[22] According to secondary ion mass spectrometry (SIMS) measurements, the mole fraction of all additive-derived impurities (C, O, S, Cl) is in the range 10^{-5} to 10^{-4}.[25, 26] Thus, while the case for incorporation is strong, there is no direct evidence that the copper films contain the glycol or some fragment derived from it. However, calculations from the model based on the assumption of inhibitor incorporation are presented here because they evaluate the implications of this assumption, which has been used in previous models of additive-assisted electrodeposition.[2]

The topography of copper electrodeposits suggests that deposition proceeds, at least in part, by independent three-dimensional growth of crystallites.[18,31] Grains are presumed to form when the side surfaces of neighboring crystallites are brought into contact by lateral growth, at which point these surfaces become grain boundaries. A simple concept for incorporation is that any additives adsorbed on the side surfaces are trapped, and that the additive coverage on grain boundaries is the same as that on the exposed surface. In the present model, the incorporated species is taken to be a PEG derivative, so this equivalent coverage assumption is made with regard to PEG. Any incorporation of the brightener, MPSA, is disregarded, since its coverage does not explicitly enter this model.

The glycol incorporation rate per unit area is

$$r_{inc} = \left(\frac{3}{R}\right)\left(\frac{Mr_2}{\rho}\right) N_{s2}\theta_2 \quad [7]$$

The first factor in parentheses is the surface area per unit volume on buried crystal grain boundaries. To a first approximation, the grains are taken as spherical with an average radius R. Since $N_{s2}\theta_2$ is the molar surface concentration of PEG, multiplying $3/R$ by this factor gives the volumetric concentration of buried PEG in the deposit. The second factor enclosed by parentheses is the volumetric deposition rate of copper per unit surface area. The assumption of a spherical grain shape is consistent with similar grain dimensions in the three coordinate directions, as observed in microscopic images of as-plated deposits.[16] If another simple grain shape such as a cylinder or slab were appropriate, the numerical factor in Eq. 7 would change from 3 to 2 (cylinders) or 1 (slabs), but the form of the expression would be the same.

Prediction of the PEG coverage additionally requires knowledge of its adsorption rate. Adsorption of dilute, slowly diffusing species such as the large PEG molecule is often controlled by their diffusion to the surface. The hypothesis of diffusion control for the glycol may be evaluated using a QCM measurement of transient mass uptake on copper due to PEG adsorption.[14] After addition of a PEG-Cl^- mixture to the solution (whose composition was nearly the same as that assumed in the present simulation), the electrode mass increased for about 2-3 s until a new steady state was attained. For diffusion-controlled adsorption, the PEG surface coverage would follow

$$\frac{d\theta_2}{dt} = \frac{D_2}{N_{s2}\delta_2}\left(C_{b2} - K\frac{\theta_2}{1 - \theta_2}\right) \quad [8]$$

This equation assumes pseudosteady diffusion and no PEG incorporation in the deposit because of the small deposition rate. The factor in parentheses is the difference between the bulk and near-surface concentrations of dissolved PEG, where the latter is in equilibrium with the PEG surface coverage according to a Langmuir isotherm. Choice of parameter values is discussed below. Numerical solution of Eq. 8 revealed that at a time of $N_{s2}\delta_2/D_2C_{b2}$, θ_2 had approached equilibrium within 5%. Using an estimate of δ_2 during the transient diffusion period to be one-half of its steady-state value of 82 μm, the adsorption time is then found to be 3 s, the same as that cited by Kelly and West. Therefore, diffusion-controlled adsorption of PEG is reasonable.

The PEG surface mole balance accounting for incorporation and diffusion-controlled adsorption is

$$N_{sp}\frac{d\theta_2}{dt} = D_2\frac{\partial C_2}{\partial x}\Big|_{x=0} - \left(\frac{3MN_{s2}k_2}{\rho R}\right) e^{-b_2 E}\theta_2\theta_3 \quad [9]$$

Downloaded on 2014-02-10 to IP 129.186.176.91 address. Redistribution subject to ECS license or copyright; see ecsdl.org/site/terms_use

As with cupric ions, transport of PEG is modeled using the concept of a stagnant diffusion layer adjacent to the surface, outside of which the solution is effectively mixed by natural convection. Transient diffusion of PEG was taken into account by solving the diffusion equation

$$\frac{\partial C_2}{\partial t} = D_2 \frac{\partial^2 C_2}{\partial x^2} \quad [10]$$

The approximation of linear concentration profiles was not made with regard to PEG because of its low diffusivity relative to cupric ions. The boundary condition for Eq. 10 at the electrode surface is

$$C_2|_{x=0} = K \frac{\theta_2}{1 - \theta_2} \quad [11]$$

Competitive adsorption model.—In the competitive adsorption model, thiol molecules adsorb slowly and irreversibly on the electrode during the potential scan, displacing PEG from the surface.[8,10,11] Since I-E curves with an adsorbed thiol monolayer are little different from those in solutions without additives,[12] the effect of this displacement is assumed to be equivalent to PEG desorption into a thiol-free solution. As done in the empirical model of competitive adsorption,[8,10] the rate of thiol adsorption is described using the kinetic model obtained for transient adsorption of alkylthiols onto gold from ethanol solutions.[32] In this study, adsorption was found to be under mixed diffusion and kinetic control, so that its rate is given by

$$r_{ads} = D_4 \frac{C_{b4} - C_4|_{x=0}}{\delta_4} = k_4 C_4|_{x=0}(1 - \theta_4) \quad [12]$$

The diffusivity of thiol in water was estimated to be 1.1×10^{-5} cm^2/s by correcting the diffusivity in ethanol,[32] using the ratio of solvent viscosities.[33] This relatively high diffusivity suggests the assumption of a linear concentration profile, as done in Eq. 12. Using Eq. 12, the surface mole balance on thiol is

$$N_{s4} \frac{d\theta_4}{dt} = k_4 C_{b4} \frac{1 - \theta_4}{1 + Da_4(1 - \theta_4)} - \frac{3MN_{s4}k_2}{\rho R} \theta_3 \theta_4 \quad [13]$$

where $Da_4 = k_4\delta_4/D_4$ is the Damköhler number for thiol adsorption. The first term on the right side accounts for adsorption, and the second incorporation of the thiol on grain boundaries. As in Eq. 7, the additive concentration on the grain boundaries and the surface are assumed to be the same. The calculated value of Da_4 of about 0.2 suggests that adsorption is determined primarily by kinetics. Exploration of diffusion-controlled adsorption using the simulation confirmed that it does not lead to realistic I-E curves.

Calculations of transient PEG adsorption during the potential scan showed that, starting with a clean electrode surface, the full PEG coverage is attained in a few seconds, at which point the thiol coverage is still very small. Hence, the initial conditions for calculations with the competitive adsorption model were equilibrium PEG coverage and zero thiol coverage. To calculate the reduction of PEG coverage during the experiment, it was assumed that a given increment of adsorbing MPSA irreversibly displaces an equivalent area coverage of PEG

$$\frac{d\theta_2}{dt} = -\frac{k_4 C_{b4}}{N_{s4}} \frac{(1 - \theta_4)\theta_2}{1 + Da_4(1 - \theta_4)} \quad [14]$$

The right side of Eq. 14 is the fractional surface area per time covered by adsorbing thiol, multiplied by the portion of that area occupied by PEG. θ_2 from Eq. 14 was used in the calculation of the copper deposition rate in Eq. 3. Note that the PEG balance neglects readsorption onto any fresh surface exposed by thiol incorporation. This issue is discussed below along with the model calculation results.

Table I. Values of model parameters used in simulation.

b_1	19.9 V^{-1}
b_2	31.0 V^{-1}
C_{b1}	2.5×10^{-4} mol/cm^3
C_{b2}	8.9×10^{-8} mol/cm^3
D_1	5.3×10^{-6} cm^2/s
D_2	1.0×10^{-6} cm^2/s
D_4	1.1×10^{-5} cm^2/s
K	2.75×10^{-9} mol/cm^3
k_1	2.0×10^{-8} cm/s
k_2	1.0×10^{-14} mol/cm^3-s
k_4	1.4×10^{-4} cm/s
N_{s3}	3.2×10^{-9} mol/cm^2
N_{s2}	5.8×10^{-11} mol/cm^2
N_{s4}	8.0×10^{-10} mol/cm^2
V_R	1 mV/s
δ_1	1.25×10^{-2} cm
δ_2	8.24×10^{-3} cm
δ_4	1.50×10^{-2} cm

Results and Discussion

Model input data.—The model input parameters are listed in Table I. The bath composition (C_{b1} and C_{b2}) and potential scan parameters (V_R, E_1, and t_R) were chosen to be the same as in experiments.[12] The kinetic parameters for copper deposition and the copper diffusion coefficient (k_1, k_2, b_1, b_2, and D_1) were set at the values chosen by Kelly and West to simulate deposition from chloride-containing acid sulfate baths either with or without PEG.[13] The PEG and MPSA diffusivities were taken from experimental measurements.[32,34] The PEG adsorption equilibrium constant was set to give an equilibrium surface coverage θ_2 of 0.97 at the bulk concentration 8.9×10^{-5} M (equivalent to 300 ppm of 3400 Mw PEG). This coverage was obtained by fitting of electrochemical impedance and steady-state polarization measurements,[13] and is consistent with mass changes due to PEG adsorption measured with QCM.[14] The PEG site density was determined considering a diam of 1.7 nm for the adsorbed molecule, obtained from a QCM study of PEG adsorption on copper.[14] The thiol site density was taken as that for closest packing, which is found to approximate measured thiol saturation coverages on gold.[32] The diffusion layer thicknesses for PEG and MPSA were found by adjusting the thickness of 125 μm determined from the limiting current for copper deposition, using the mass transport correlation for natural convection.[35] The model differential equations were integrated numerically with the help of subroutine D03PHF in the Numerical Algorithms Group Fortran library (Oxford, U.K.).

Results of calculations with PEG incorporation model.—Figure 2 shows simulated I-E curves for deposition of ''large grain'' copper from PEG-free baths and PEG-containing baths. Also shown are results for PEG-containing baths, in which the grain diameter was taken as 1 μm or 100 nm. All baths are assumed to contain 0.25 M $CuSO_4$ and 1.8 M H_2SO_4, as well as 1 mM chloride ions. The ''large grain'' deposits were produced in the model by setting the grain radius to 5 cm, so that the rate of incorporation of PEG at grain boundaries is negligible. The grain diam of 100 nm is characteristic of deposits formed in three-additive baths with thiols in addition to PEG and chloride ions.[15-17] In the PEG incorporation model, the only effect of MPSA is assumed to be grain refinement. Plots of PEG fractional surface coverage *vs.* potential for the simulations in Fig. 2 are shown in Fig. 3.

In Fig. 2, the curve for large grain deposits in PEG baths is shifted from the no-PEG curve by about −150 mV, as a result of the inhibiting effect of the glycol on deposition. For current densities below 20 mA/cm^2, I-E curves in solutions with no additives are closely similar to those with chloride as the only additive.[14] Thus,

Downloaded on 2014-02-10 to IP 129.186.176.91 address. Redistribution subject to ECS license or copyright; see ecsdl.org/site/terms_use

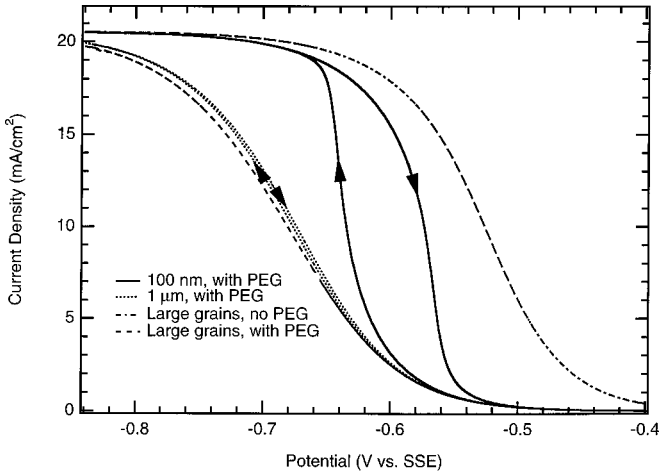

Figure 2. I-E scans simulated by PEG incorporation model, showing the effect of PEG addition and deposit grain diameter (numerical parameter in legend).

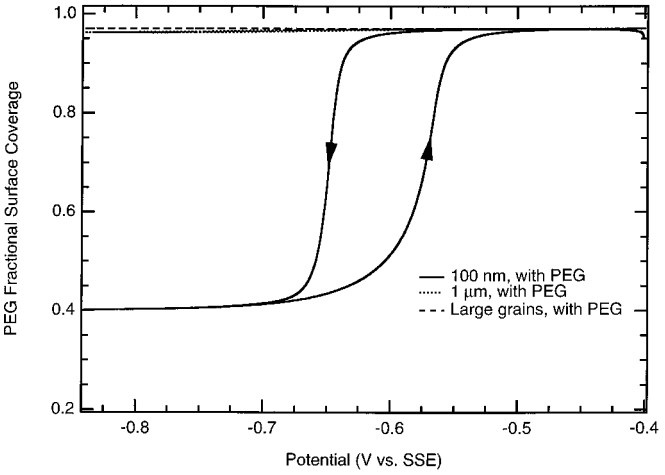

Figure 3. PEG fractional surface coverage *vs.* potential for the same simulation runs in Fig. 2.

the no additives curve in Fig. 1 can be considered approximately the same as one in a bath with chloride but no PEG. This curve, and the Cl-PEG curve in Fig. 1, are quantitatively similar to the corresponding model I-E curves in Fig. 2. This agreement is not surprising, since the ability of this kinetic model to simulate steady-state I-E curves in these solutions has been documented.[13]

Hysteresis begins to appear when the grain diameter is reduced to 1 μm, but the hysteresis loop is no wider than 10 mV. Voltage traces in both the positive and negative directions lie close to the PEG-chloride curve, indicating that deposition is still strongly inhibited, consistent with the high surface coverage in Fig. 3. Upon reducing the grain diameter further to 100 nm, the I-E curve shifts strongly toward positive potentials and the hysteresis increases. The shift of the negative-going potential trace is as much as 150 mV. The location of this trace along the potential axis compares favorably to the chloride-PEG-MPSA curve in Fig. 1: for example, the potentials at 10 mA/cm^2 differ by less than 10 mV. The hysteresis in the predicted I-E curve is about 60 mV along the potential axis, compared to the experimental hysteresis of 100 mV in the three-additive bath. In both model and experimental hysteresis loops, higher currents are found during the return scan toward positive potentials.

The origin of hysteresis in the PEG incorporation model may be understood with regard to Fig. 2 and 3. The activation of deposition during the initial cathodic scan begins when the current density on the surface with high PEG coverage is large enough so that the magnitude of the incorporation rate in Eq. 9 is comparable to the adsorption rate. The coverage of PEG then begins to decrease, and continues to do so until a steady-state coverage of 0.40 is reached at the limiting current plateau. On the anodic return scan, the PEG coverage begins to increase when the current falls below the limiting value. The transition between high and low coverages occurs at a more anodic potential in the return scan, owing to the enhanced deposition kinetics at the lower PEG coverage present during this scan. Referring to Eq. 9, the transition potentials are those where the adsorption and incorporation terms are approximately equivalent, for either inhibited or activated deposition kinetics.

The predicted mole fraction of PEG is $3N_{s2}\theta_2 M/\rho R$, which, using a fractional coverage of 0.40 and a grain radius of 50 nm, is found to be 1×10^{-4}. Since each PEG molecule contains 150 carbon atoms, this corresponds to a carbon mole fraction of order 10^{-2} in the deposit. This is much higher than the impurity mole fractions measured experimentally, which range from 10^{-5} to 10^{-3} mole fraction.[22,25,26] The overprediction of the carbon content can only be reconciled if extensive diffusion of the glycol out of the deposit occurred prior to the composition measurements, a possibility regarded as perhaps unlikely. Therefore, the low impurity content of deposits appears to be inconsistent with the incorporation rate of PEG needed to effectively remove the adsorbed inhibitor from the surface, producing the observed I-E hysteresis.

Results of calculations with competitive adsorption model.—The I-E curves generated by this model are presented in Fig. 4. The bulk MPSA concentrations were chosen to be the same as those in voltammetry experiments.[8] As in the experiments, I-E hysteresis is present for all three MPSA concentrations. The locations of experimental and model voltammetry curves on the potential axis can be compared using the same current density of 10 mA/cm^2. In the cathodic direction scan, the potentials in Fig. 4 at this current density are −0.68, −0.64, −0.59, and −0.57 V in order of ascending thiol concentration, and the corresponding experimental potentials are −0.73, −0.67, −0.60, and −0.57 V.[8] For the anodic direction scans, the potentials at 10 mA/cm^2 in Fig. 4 in the thiol-containing baths are −0.61, −0.55, and −0.53 V in order of increasing concentration, compared to −0.55, −0.53, and −0.52 V from the experimental curves. Thus, the positions of the cathodic scans in thiol baths agree reasonably with experiment, as do those of the anodic scans with the exception of the lowest thiol concentration of 1.26 μM. During the cathodic scan, the rate of adsorption of thiol determines the time and potential at which the removal of PEG causes the

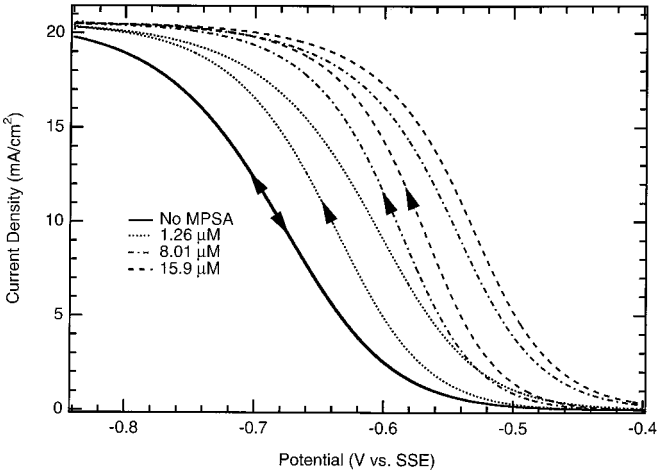

Figure 4. I-E scans simulated by competitive adsorption model. Parameter is MPSA bulk concentration.

Downloaded on 2014-02-10 to IP 129.186.176.91 address. Redistribution subject to ECS license or copyright; see ecsdl.org/site/terms_use

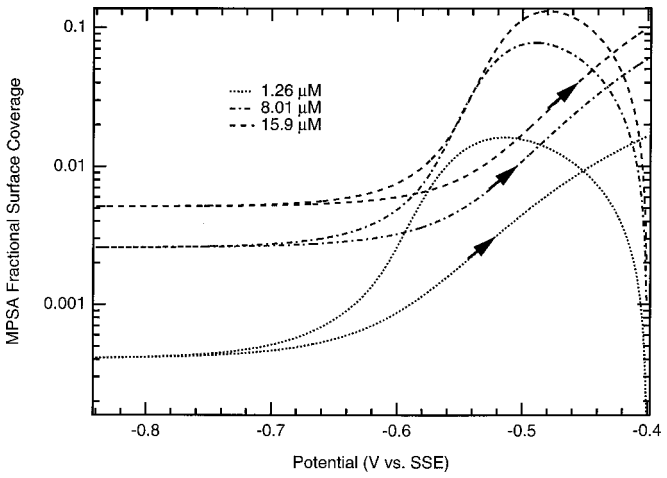

Figure 5. MPSA fractional surface coverage *vs.* potential for the simulation runs in Fig. 4. Parameter is MPSA bulk concentration.

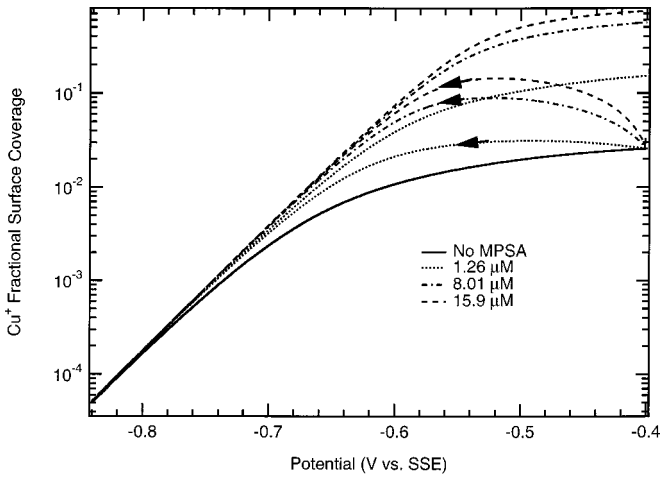

Figure 7. Cuprous ion fraction surface coverage *vs.* potential for the simulation runs in Fig. 4. Parameter is MPSA bulk concentration.

current to rise steeply. The ability to predict this potential is then evidence that thiol adsorption was modeled properly.

Plots of thiol coverage *vs.* potential (Fig. 5) demonstrate that the adsorption of MPSA leads to a gradually increasing coverage during the cathodic-direction scan, until current densities of approximately 1 mA/cm^2 are attained. At this point, the rate of incorporation becomes significant, and as the current continues to rise the MPSA coverage falls to values of 10^{-4} to 10^{-2}. The low predicted thiol coverage during activated deposition is due to the much larger plating rate compared to that of MPSA adsorption. A relevant experiment was reported by Eliadis *et al.*, who used X-ray photoelectron spectroscopy (XPS) to detect adsorbed pentanethiol on gold electrodes prior to and after electrodeposition of copper.[36] The spectra before but not after deposition showed the presence of thiol; however, the thiol reappeared after anodic stripping of copper, suggesting that it had been buried beneath the deposit surface. The correlation of low thiol coverage during deposition with incorporation into the copper film is the same as in the model predictions.

The behavior of PEG and cuprous ions during the simulation is illustrated in Fig. 6 and 7, respectively. The PEG coverage decreases monotonically during the entire potential scan, due to continuing thiol adsorption which displaces it from the surface. The Cu^+ ion coverage is between 0.02 and 0.1 at potentials more positive than −0.6 V, but decreases exponentially at more negative potentials during the cathodic-direction trace. This potential dependence is due to the larger charge transfer coefficient of Cu^+ reduction to Cu (Eq. 2), compared to that of Cu^{+2} reduction to Cu^+ (Eq. 1). During the return scan, the cuprous ion coverage increases again, reaching values greater than 0.1 at potentials above −0.6 V. It is apparent that the Cu^+ coverage is negligible when the current density is about 10 mA/cm^2 or larger, but not so at low current densities around 1 mA/cm^2.

Since the thiol coverage is very low when the deposition kinetics are activated, it is important to consider whether readsorption of PEG can occur. The simulation of Fig. 5-7 does not account for this effect, and it predicts activation of the copper surface and hysteresis similar to those found experimentally. In order to explore readsorption, a diffusion-limited adsorption term was appended to the PEG surface mole balance, Eq. 14. This term was the same as that in the PEG incorporation model (Eq. 9). The I-E curves generated by the modified simulation are shown in Fig. 8. For all MPSA bath concentrations, the curves lie close to the one for the PEG-chloride bath, indicating that no activation of copper deposition occurs. In these calculations, readsorption causes the PEG coverage to remain high, in spite of the continuing displacement of PEG by thiol. Since, in contrast to Fig. 8, activation and hysteresis are clearly evident in the experimental I-E curves, it is suggested that readsorption of PEG

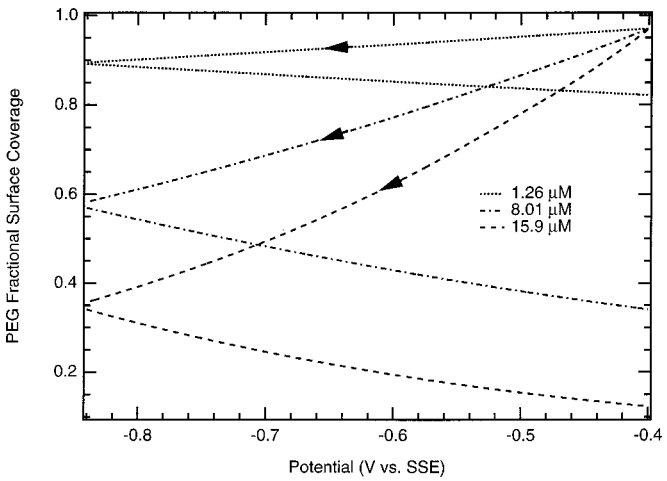

Figure 6. PEG fractional surface coverage *vs.* potential for the simulation runs in Fig. 4. Parameter is MPSA bulk concentration.

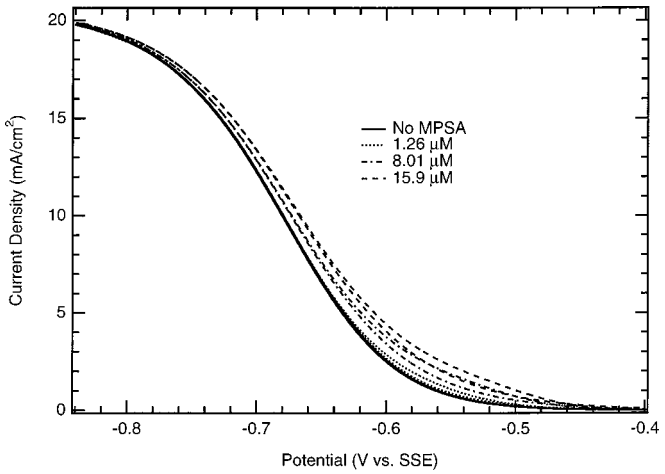

Figure 8. I-E scans simulated by competitive adsorption model, with the addition of an adsorption term to the PEG surface mole balance (Eq. 14). Parameter is MPSA bulk concentration.

Downloaded on 2014-02-10 to IP 129.186.176.91 address. Redistribution subject to ECS license or copyright; see ecsdl.org/site/terms_use

does not occur in the experimental system. A possible reason is indicated by the low cuprous ion coverage in the presence of high deposition currents (Fig. 7). It has been proposed that PEG bonds to the copper surface by means of a Cu^{+}-Cl^{-} linkage.[37] This concept is supported by the chemical affinity of cuprous ion for both the ether oxygen of PEG and chloride ions,[38] which in turn strongly adsorb on copper in the potential region under consideration.[39] Therefore, since adsorbed Cu^{+} ions may be necessary for bonding of PEG to the surface, the latter may not occur at high deposition current owing to the low cuprous ion coverage. The glycol could still be loosely attached to the metal surface, as suggested by Raman spectroscopy results,[40] but would not inhibit deposition due to the lack of secure bonding through adsorbed Cu^{+} ions.

The mole fractions of carbon and sulfur in the deposit according to the competitive adsorption model are determined by the mole fraction of incorporated thiol, $3N_{s4}\theta_4 M/\rho R$. For the MPSA concentrations of 1.26, 8.01, and 15.9 μM, the C mole fractions are 3×10^{-6}, 2×10^{-5}, and 6×10^{-5}, while the S mole fractions are 2×10^{-6}, 1×10^{-5}, and 4×10^{-5}. Thus, assuming that industrial baths contain about 10 μM thiol, the C and S mole fractions should be between 10^{-5} and 10^{-4}, the same order of magnitude found by SIMS.[26,27] This point of agreement with the experiment is encouraging evidence supporting the treatments of thiol adsorption and incorporation in the model. In particular, the presence of thiol-derived C and S throughout the deposit indicates that thiol adsorbs continuously during deposition, for which it is necessary that its surface coverage is maintained at small values, consistent with the model predictions. No prior simulation is known to have predicted realistic concentrations of additive-derived impurities in the deposit.

As pointed out above, the most evident discrepancy between simulated and experimental voltammograms is that, for the lowest MPSA concentration, the model I-E curve during the anodic direction scan is shifted toward negative potentials relative to the experimental curve. The more positive potential of the experimental trace suggests a greater displacement of PEG from the surface. However, the discrepancy in I-E curves may arise not from slow thiol adsorption, but because the number of thiol molecules needed to displace a large PEG molecule is smaller than that suggested by Eq. 14. Even with this tendency to underpredict the displacement of glycol, the rate of removal of PEG for the two highest MPSA concentrations is sufficient to activate deposition during the anodic potential scan, and to produce agreement with the experimental I-E traces.

To summarize, the present competitive adsorption model yields a promising agreement with experimental I-E curves, as well as with SIMS measurements of incorporated carbon and sulfur. The absence of fit parameters is in contrast to other simulations,[8-10] and gives encouragement that models can be developed which are able to predict deposition behavior over a wide range of conditions. According to the simulation results, deposition is inhibited by adsorbed PEG, and is activated by adsorbing thiol which displaces PEG from the surface. Since the resulting deposition rate far exceeds that of MPSA adsorption, the thiol is incorporated in the deposit and depleted from the surface. Evidently, readsorption of PEG onto the copper does not occur while the deposition rate is large, possibly because of the absence of adsorbed cuprous ions which are necessary to bond PEG.

Conclusions

Models were formulated for linear sweep voltammetry experiments carried out during electrodeposition of copper from baths with PEG, chloride, and thiol additives. The deposition kinetics in the models followed those determined for PEG-chloride baths.[13] Two models were tested which assumed different mechanisms for removal of the PEG inhibitor from the surface: incorporation into the deposit, or displacement by adsorbed thiol. Unlike previous simulations of similar experiments,[8-10] the equations and parameters of the each model were obtained from independent sources.

The I-E curves predicted by the PEG incorporation model showed hysteresis similar to experiments only when a grain size as small as 100 nm was chosen. While such small grain sizes are typical of actual deposits, the predicted concentration of incorporated additive for these conditions was excessive relative to experimental measurements. The competitive adsorption model also yielded realistic I-E curves with hysteresis, and in addition carbon and sulfur concentrations in the deposit compared well with measurements. The level of agreement of this model with voltammograms was similar to that of empirical models based on competitive adsorption,[8,10] which have further demonstrated the capability to simulate superfilling of cavities. However, such models may not be suitable for prediction of deposition with different bath compositions from those for which fitting was carried out. In order to improve and further validate the present model, the details of PEG and thiol adsorption should be investigated further.

Acknowledgments

Helpful discussions with Dr. K. M. Takahashi (Agere Systems) are gratefully acknowledged.

List of Symbols

b_1, b_2	Tafel coefficients for copper deposition, V^{-1}
C_1, C_2, C_4	Cu^{+2}, PEG, and MPSA concentrations, mol/cm^3
C_{b1}, C_{b2}, C_{b4}	Cu^{+2}, PEG, and MPSA bulk concentrations, mol/cm^3
D_1, D_2, D_4	Cu^{+2}, PEG, and MPSA diffusion coefficients, cm^2/s
E_1	initial potential in CV experiment, V
K	adsorption equilibrium constant, mol/cm^3
k_1	rate constants for Cu^{+2} reduction to Cu^{+}, cm/s
k_2	rate constant for Cu^{+} reduction to Cu, mol/cm^2-s
k_4	MPSA adsorption rate constant
E	Potential, V *vs.* saturated sulfate electrode
F	Faraday constant, 9.64767 C/equiv
i_d	copper deposition current density, A/cm^2
M	atomic mass of copper, g/mol
N_{s3}, N_{s2}, N_{s4}	Cu^{+}, PEG, and MPSA adsorption site density, mol/cm^2
R	radius of deposited crystal grain, cm
t	time, s
t_R	scan reversal time, s
V_R	voltage ramp rate, V/s
x	position coordinate measured from electrode surface, cm

Greek

δ_1, δ_2, δ_4	diffusion layer thickness for Cu^{+2}, PEG, and MPSA, cm
θ_2, θ_3, θ_4	fractional surface coverages of PEG, Cu^{+1}, and MPSA
ρ	density of copper, g/cm^3

References

1. P. C. Andricacos, C. Uzoh, J. O. Dukovic, J. Horkans, and H. Deligianni, *IBM J. Res. Dev.*, **42**, 567 (1998).
2. K. G. Jordan and C. W. Tobias, *J. Electrochem. Soc.*, **138**, 1251 (1991).
3. J. O. Dukovic, *IBM J. Res. Dev.*, **37**, 125 (1993).
4. D. Roha and U. Landau, *J. Electrochem. Soc.*, **137**, 824 (1990).
5. C. Madore, M. Matlosz, and D. Landolt, *J. Electrochem. Soc.*, **143**, 3927 (1996).
6. A. C. West, *J. Electrochem. Soc.*, **147**, 227 (2000).
7. M. Georgiadou, D. Veyret, R. L. Sani, and R. C. Alkire, *J. Electrochem. Soc.*, **148**, C54 (2001).
8. T. P. Moffat, D. Wheeler, W. H. Huber, and D. Jossell, *Electrochem. Solid-State Lett.*, **4**, C26 (2001).
9. A. C. West, S. Mayer, and J. Reid, *Electrochem. Solid-State Lett.*, **4**, C50 (2001).
10. D. Jossell, D. Wheeler, W. H. Huber, and T. P. Moffat, *Phys. Rev. Lett.*, **87**, 16102 (2001).
11. J. Reid and S. Mayer, in *Advanced Metallization Conference 1999*, M. E. Gross, T. Gessner, N. Kobayashi, and Y. Yasuda, Editors, p. 53, Materials Research Society, Warrendale, PA (2000).
12. T. P. Moffat, J. E. Bonevich, W. H. Huber, A. Stanishevsky, D. R. Kelly, G. R. Stafford, and D. Jossell, *J. Electrochem. Soc.*, **147**, 4524 (2000).
13. J. J. Kelly and A. C. West, *J. Electrochem. Soc.*, **145**, 3477 (1998).
14. J. J. Kelly and A. C. West, *J. Electrochem. Soc.*, **145**, 3472 (1998).
15. G. Lingk and M. E. Gross, *J. Appl. Phys.*, **84**, 5547 (1998).
16. S. H. Brongersma, E Richard, I. Vervoort, H. Bender, W. Vandervorst, S. Lagrange, G. Beyer, and K. Maex, *J. Appl. Phys.*, **86**, 3642 (1999).
17. J. M. E. Harper, C. Cabral, P. C. Andricacos, L. Gignac, I. C. Noyan, K. P. Rodbell, and C. K. Hu, *J. Appl. Phys.*, **86**, 2516 (1999).
18. J. J. Kelly, C. Tian, and A. C. West, *J. Electrochem. Soc.*, **146**, 2540 (1999).
19. E. Mattsson and J. O'M. Bockris, *Trans. Faraday Soc.*, **55**, 1586 (1959).
20. J. O'M. Bockris and M. Enyo, *Trans. Faraday Soc.*, **58**, 1187 (1962).
21. O. R. Brown and H. R. Thirsk, *Electrochim. Acta*, **10**, 383 (1965).
22. D. Stoychev, I. Vitanova, R. Buyukliev, N. Petkova, I. Popova, and I. Pojarliev, *J. Appl. Electrochem.*, **22**, 987 (1992).
23. T. Y. B. Leung, M. Kang, B. F. Corry, and A. A. Gewirth, *J. Electrochem. Soc.*, **147**, 3326 (2000).

Downloaded on 2014-02-10 to IP 129.186.176.91 address. Redistribution subject to ECS license or copyright; see ecsdl.org/site/terms_use

24. D. R. Turner and G. R. Johnson, *J. Electrochem. Soc.*, **109**, 798 (1962).
25. S. G. Malhotra, P. S. Locke, A. H. Simon, J. Fluegel, C. Parks, P. Dehaven, D. G. Hemmes, R. Jackson, and E. Patton, in *Advanced Metallization Conference 1999*, M. E. Gross, T. Gessner, N. Kobayashi, and Y. Yasuda, Editors, p. 77, Materials Research Society, Warrendale, PA (2000).
26. M. E. Gross, R. Drese, D. Golovin, W. L. Brown, C. Lingk, S. Merchant, and M. Oh, in *Advanced Metallization Conference 1999*, M. E. Gross, T. Gessner, N. Kobayashi, and Y. Yasuda, Editors, p. 85, Materials Research Society, Warrendale, PA (2000).
27. S. Lagrange, S. H. Brongersma, M. Judelewicz, A. Saerens, I. Vervoort, E. Richard, R. Palmans, and K. Maex, *Microelectron. Eng.*, **50**, 449 (2000).
28. R. Walker and R. C. Benn, *Electrochim. Acta*, **16**, 1081 (1971).
29. D. S. Stoychev, I. V. Tomov, and I. B. Vitanova, *J. Appl. Electrochem.*, **15**, 879 (1985).
30. A. Gangulee, *J. Appl. Phys.*, **43**, 867 (1972).
31. R. Winand, *Electrochim. Acta*, **39**, 1091 (1994).
32. L. S. Jung and C. T. Campbell, *Phys. Rev. Lett.*, **84**, 5164 (2000).
33. E. L. Cussler, *Diffusion: Mass Transfer in Fluid Systems*, p. 118, Cambridge University Press, Cambridge (1984).
34. L. Masaro, X. X. Zhu, and P. M. Macdonald, *Macromolecules*, **31**, 3880 (1998).
35. C. R. Wilke, M. Eisenberg, and C. W. Tobias, *J. Electrochem. Soc.*, **100**, 513 (1953).
36. E. D. Eliadis, R. G. Nuzzo, A A. Gewirth, and R. C. Alkire, *J. Electrochem. Soc.*, **144**, 96 (1997).
37. M. Yokoi, S. Konishi, and T. Hayashi, *Denki Kagaku oyobi Kogyo Butsuri Kagaku*, **52**, 218 (1984).
38. D. Stoychev and C. Tsvetanov, *J. Appl. Electrochem.*, **26**, 741 (1996).
39. M. R. Vogt, A. Lachenwitzer, O. M. Magnussen, and R. J. Behm, *Surf. Sci.*, **399**, 49 (1998).
40. J. P. Healy, D. Pletcher, and M. Goodenough, *J. Electroanal. Chem.*, **338**, 155 (1992).

Downloaded on 2014-02-10 to IP 129.186.176.91 address. Redistribution subject to ECS license or copyright; see ecsdl.org/site/terms_use